J Mater Sci (2023) 58:2456–2468

Ceramics

In-situ scanning transmission electron microscopy study of Al-amorphous SiO_2 layer-SiC interface

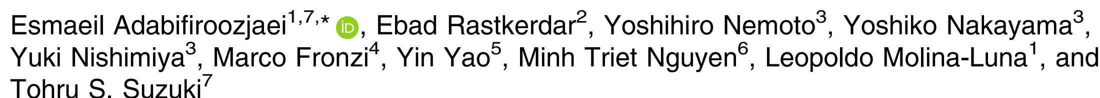

Esmaeil Adabifiroozjaei[1,7,*], Ebad Rastkerdar[2], Yoshihiro Nemoto[3], Yoshiko Nakayama[3], Yuki Nishimiya[3], Marco Fronzi[4], Yin Yao[5], Minh Triet Nguyen[6], Leopoldo Molina-Luna[1], and Tohru S. Suzuki[7]

[1] *Advanced Electron Microscopy (AEM) Division, Institute of Materials Science, Technische Universität Darmstadt, 64287 Darmstadt, Germany*
[2] *Faculty of Mechanical Engineering, Department of Materials Engineering, University of Tabriz, Tabriz 5166616471, Iran*
[3] *Electron Microscopy Analysis Station, Nanostructural Characterization Group, National Institute for Materials Science (NIMS), Tsukuba 305-0047, Japan*
[4] *IGP, SIT Laboratory, College of Engineering, Shibaura Institute of Technology, Tokyo 135-8548, Japan*
[5] *Electron Microscopy Unit (EMU), UNSW Sydney, Mark Wainwright Analytical Centre, Sydney, NSW 2052, Australia*
[6] *ARC Center of Excellence in Exiton Science, School of Physics, UNSW Sydney, Sydney, NSW 2052, Australia*
[7] *Research Center for Functional Materials (RCFM), National Institute for Materials Science (NIMS), Tsukuba 305-0047, Japan*

Received: 18 August 2022
Accepted: 11 January 2023
Published online: 23 January 2023

© The Author(s) 2023

ABSTRACT

Here, we present a comprehensive study on atomic-scale in-situ biasing/heating scanning transmission electron microscopy ((S)TEM) of Al-amorphous SiO_2–SiC interface. The investigation includes electrical, chemical, and structural analysis of the interface at different temperatures (25–600 °C). The results show that at $\sim$ 500 °C the electrical (three-orders of magnitude resistivity drop), chemical (dissolution of SiO_2 amorphous layer), and microstructural features (*e.g.* formation of Al_2O_3, Si and Al_4C_3) of the interface start to change. According to the results, amorphous SiO_2 dissolves in Al, leading to formation of α-Al_2O_3 and Si within the Al. In contrast, elemental interdiffusion ($Al^{3+} \rightleftarrows Si^{4+}$) between Al and SiC occurs resulting in formation of Al_4C_3. From the results, we can infer that reaction mechanism between Al and crystalline SiC is different with that between Al and SiO_2 amorphous phase. It is believed that structural similarities between SiC and Al_4C_3 play an important role in paving the way for elemental interdiffusion.

Handling Editor: N. Ravishankar.

Address correspondence to E-mail: e.adabifiroozjaei@aem.tu-darmstadt.de

https://doi.org/10.1007/s10853-023-08186-z

Introduction

The development of materials based on novel hybrid structures, particularly those containing both metals and ceramics are of great importance in today's rapidly evolving microelectronic and manufacturing industries [1, 2]. This is because by combining the different features of the metals and the ceramics (*e.g.* ductility *v.s.* brittleness, conductivity *v.s.* insulating (or semiconductor) [3]), the resulting composite material could have remarkably-improved and well-balanced properties [4–7]. Additionally, when the device is made of non-oxides (carbides or nitrides), there is an amorphous oxide layer (hereafter called AOL) between the metal and the ceramic that can potentially alter the device properties [8, 9]. Examples are, but not limited to, metal-SiC Schottky diodes [10], metal-oxide semiconductor (MOS) devices [11, 12], and metal matrix composites reinforced with non-oxides (*e.g.* SiC, TiC) [13]. One representative system that can be applied in all these applications is Al–SiC, in which AOL (few nanometers thin of amorphous SiO_2) always exist between Al and SiC [10, 11, 14–16]. In semiconductor devices, an annealing process at intermediate temperature is prescribed in order to make a closer contact between the metal and the ceramic component [14, 17], so as to adjust the electrical characteristics of the device [18–20]. Similar processes can be applied to Al–SiC composites, in which the annealing process enhances the composite mechanical properties by preventing direct contact between Al and SiC, which in turn stops the formation of brittle and undesired aluminum carbide phase (Al_4C_3) [15, 16, 21].

In spite of the central influence of the AOL on the metal-ceramic device properties, the mechanism of interaction of AOL, or the crystalline ceramic (SiC) with the reactive metal (Al) under the heat-treatment process is still not well-understood. Currently, there are two theories: (1) First theory suggests that amorphous and crystalline ceramics, regardless of their crystallinity, react with the metals through a similar mechanism, being ceramic dissolution into the metal (solid or liquid) and consequent crystallization of reaction product [20, 22, 23]. This is based on very limited dissolution of the reactive metal in the ceramics, which itself is according to equilibrium phase diagram of the relevant bulk system (*e.g.* Al–Si–C ternary system [24]). However, it is well-known that for interfaces in multicomponent systems, due to the significant role of interfacial energies, a new equilibrium system different than that of existing in the bulk systems can be observed (formation of metastable complexions in various materials [25–27]). Additionally, the reactive metal-ceramic systems are very far from the chemical equilibrium, and accordingly their behavior can deviate considerably from the systems at equilibrium [28, 29]. Also, it has to be considered that decomposition of the covalent crystalline ceramics such as SiC requires substantial amount of energy and only occurs at high temperatures (at least 1000 °C) [30, 31], which are not comparable with the heat treatment temperatures of the Al–SiC composites ($\sim$ 500–650 °C) [16, 32]. In contrast to first theory, the second theory is based on interdiffusion of elements across the interface of the metal and the ceramic. This theory was applied in the previous works on Al–Si_3N_4 [33], Al–$CaAl_2Si_2O_8$ [34, 35], Al–$BaAl_2Si_2O_8$ [36, 37], and Al–$MgAl_2O_4$ [38] systems, in which elemental interdiffusion (*e.g.* $Al^{3+} \rightleftarrows Ca^{2+}$, $Al^{3+} \rightleftarrows Si^{4+}$, $Al^{3+} \rightleftarrows Mg^{2+}$) across the metal-ceramic interface was proposed as the interfacial phase evolution mechanism. Furthermore, the $Al^{3+} \rightleftarrows Si^{4+}$ interdiffusion was also considered in the past as the mechanism of interfacial phase evolution in the Al–SiC system, but due to the resolution limit (10 nm) of the microscopes, this mechanism was not confirmed [32]. Furthermore, recent studies on metal-ceramic interfaces showed that rate of elemental interdiffusion at the interface can be a few orders of magnitude higher than that observed in the bulk ceramics [1, 39]. The major issue is that the studies conducted so far, regardless of the mechanism proposed in them, were ex-situ and expectedly not being capable of resolving the atomic-scale nanostructural and chemical changes occurring at the interfaces during the heat-treatment process. Hence, there is still ambiguity in understanding of how reactive metal-ceramic interfaces evolve when exposed to high temperature.

Here, by the application of atomic resolution, in-situ (S)TEM techniques (using Cs corrected microscopes) we reveal the evolution mechanism of the Al–AOL–SiC system under biasing/heating conditions. Our I–V curves and high resolution TEM (HRTEM) images acquired from in-situ biasing/heating test at different temperatures indicate that the resistivity of the Al–AOL–SiC device decreased three orders of magnitudes at 500 °C with no apparent change in the

nanostructure. Separate in-situ heating experiment with acquisition of the STEM-HADDF (high-angle annular dark field) images and interfacial chemical profile (using EELS (energy electron loss spectroscopy)) of the elements show that at 550 °C the AOL width was reduced, which was due to AOL dissolution into the Al. The structural analysis of the interface at 600 °C confirms formation of Al_2O_3 and Si in the Al, but Al_4C_3 within the SiC with no clear boundary. Structural similarities of Al_4C_3 and SiC as well as the lack of observation of SiC dissolution into the metal lead us to conclude that elemental interdiffusion ($Al^{3+} \leftrightarrows Si^{4+}$) between Al and SiC results in topotactic formation of Al_4C_3 from SiC as a precursor.

Experimental

4H n-type SiC wafer with thickness of ~ 350 µm was purchased from Electronics and Materials Corporation Limited (Hyogo, Japan)). The growth direction of SiC wafer was [0001]. The main impurity in SiC was nitrogen with calculated content of 1×10^{19} atom/cm^3. The wafer was ultrasonically cleaned in acetone for few mins and then was dipped into 10 wt% HF solution for 5 min to remove the oxide layer present on SiC. Immediately after removal of the oxide layer, the SiC wafer was put in desiccator for few days in order to allow the regrowth of the oxide layer. Then, an Al layer with thickness of ~ 1 µm was sputtered on the wafer. In order to decrease heating caused from sputtering process, very low sputtering speed (~ 1.85 Å/s) was used. The sputtering was applied using an i-miller stutterer (CFS-4EP-LL, Shibaura Mechatronics Corporation, Yokohama, Japan). Focused ion beam (JIB-4000, JEOL Ltd., Tokyo, Japan and JEM-9310FIB, JEOL Ltd., Tokyo, Japan) milling was used to prepare the lamellae. Similar lamellae were prepared, some of which was used for in-situ biasing/heating experiment and the other ones for in-situ heating. DENSsolutions lightning nano-chip was used for in-situ biasing/heating experiment (Fig. 1a). The prepared lamella was loaded on the chip using micromanipulator. The low- and high-magnification scanning electron microscopy (SEM) images of the chip and the loaded lamella are shown in Fig. 1b, c. Lamella was glued to chip using epoxy resin. Then, two Au lamellae were prepared by FIB and connected to Al–AOL–SiC lamella and chip. This was to ensure electrical current passes through Al–AOL–SiC lamella. No glue was used for connection of Au lamellae and Al–AOL–SiC lamella. For in-situ heating experiment DENSsolutions nano-chip was used (Fig. 1d). The low- and high-magnification optical microscopy (OM) images of the chip and the loaded lamella are shown in Fig. 1e, f. Here, only epoxy was used to ensure that the lamellae is tightly bonded to the chip.

For the in-situ biasing/heating experiment, a DENSsolutions Lightning holder (DENSsolutions B.V., Delft, The Netherlands) was used. To regulate the heating and biasing, both DENSsolutions Lightning heating and Protochips Fusion electric biasing systems (Protochips Inc., Morrisville, NC, USA) were used. The prepared lamella was loaded on a DENSsolutions Lightning chip, and a compliance current of 3 nA was applied. Then the voltage required to reach such a current was recorded at each temperature. The temperature was increased from room temperature to 600 °C with an interval of 100 °C and holding time of 30 min at each temperature. Between 500 and 600 °C the interval was set to 50 °C. The I–V curves were measured at each temperature over the holding time and any changes or variations were recorded. After finishing the characterization at 600 °C, the sample was cooled down to room temperature. The change in the microstructure of the interface was recorded in TEM mode by imaging and capturing movies. For imaging, $1\bar{1}00$ zone axis was chosen for SiC single crystal. Since sputtered Al is formed as polycrystalline, closest zone axis of a grain of Al to $1\bar{1}00$ zone axis of SiC was found and all analysis were done accordingly.

In-situ heating test was done using the same holder, but on a DENS solutions Wildfire chip. Heating procedure was same as biasing/heating test. Microstructural analysis was done in the STEM mode. EELS was conducted to measure the chemical profile of the different elements across the interface. The resolution of the EELS line analysis was 4 Å. K-edges of Al, Si, O, and C were used in order to acquire the chemical profiles. Same edges were used for obtaining elemental maps, however, elemental mapping seemed to damage/change the lamella. Therefore, the chemical changes occurring at the interface were only characterized using the line chemical profiles acquired from EELS. At each temperature, the line profile measurements were recorded. In order to record the change in the

microstructure, HAADF (High-Angle Annular Dark Field) imaging was done at each temperature. The imaging was done when holding time was over. EDS mapping measurements was also done to characterize the AOL layer before doing the tests. The thickness of lamellae was measured using EELS. The in-situ tests were done using JEM-ARM200F (Cold FEG and 2 Cs correctors (CL and OL)) machine (JEOL Ltd. Tokyo, Japan).

Results

Before starting the in-situ tests, the microstructure and the thickness of the lamellae were studied, as they are important factors in obtaining high quality in-situ TEM data. Figure 2a shows a low-mag bright field TEM image of a prepared lamella. The middle part of lamella was further thinned compared to the sides, as this would be the area of interest. No bending contours are observed in the "analyzed area", indicating a high-quality lamella. Figure 2b shows a STEM image of a small part of the analyzed area, showing the Al–AOL–SiC interface. The graphic plot shows the variation of thickness of the lamella across the interface. The thickness of the SiC part of the lamella is ~ 100 nm, while that on Al side is ~ 80 nm.

The chemical composition of the phases across the Al–AOL–SiC interface was also studied. EDS mapping of the interface is shown as Fig. 3a, while high resolution EELS elemental mapping of the interface is given as Fig. 3b. In Fig. 3a, b, the presence of a narrow layer of oxide layer is visible. The thickness of the layer is in the range of 3–5 nm and it is consistently present everywhere along the interface. As seen from the EELS chemical profile, the layer does not have a sharp profile, meaning that the layer is not pure SiO_2.

The electrical characteristics of the lamella was studied using the in-situ biasing/heating TEM test. The acquired I–V curves for room temperature, 500 ° and 600 °C after 30 min of application of the field are presented in Fig. 4a–c, respectively. The curves for 100 ° and 400 °C are presented as Fig. S1. The applied compliance current was set to 3 nA (vertical axis) and accordingly the voltage (horizontal axis) required to reach to such current was recorded at each temperature. As seen, the voltage required to reach the set current is same for temperatures lower than 500 °C, while at this temperature it decreases drastically (three orders of magnitude) and stays the same at 600 °C. Since the current is set, the decrease in voltage implies that the resistivity of the device is decreased in same orders of magnitude as the decrease in the voltage. The resistivity reduction possibly implies to closer contact of the Al and SiC, meaning that AOL width was reduced or alternatively the AOL layer was locally removed through the interfacial reaction with the metal. Such situation will result in change of chemical bonding of the phases involved at the interface [14, 17, 18]. To evaluate the nanostructure of the Al–AOL–SiC interface, the HRTEM images of investigated area of the interface are given as Fig. 4 d–f for room temperature, 500 ° and 600 °C, respectively. The FFT of the HRTEM images is also presented as insets in these figures (see low-magnification images in Fig. S2). Low- and high-magnification TEM images of the device at 100 ° and 400 °C are also shown as Fig. S3. The HRTEM images and related FFTs do not indicate significant changes in the interface nanostructure, particularly the hallow pattern of the amorphous layer stays the same over the heat-treatment process. Since the length of the interface in the lamella is ~ 15 µm, there is a high chance that the expected structural changes occurred at other points of the interface and therefore were missed in our observation. To explore the possibility, two movies (Movie S1: low-magnification, and Movie S2: high-magnification) were captured along the interface at 600 °C. But, no significant changes were observed in the structure of the AOL. Another reason for missing the structural changes could be that the experiment was done in TEM mode, which is a phase contrast imaging mode and obviously being focus-dependent. Moreover, since the experiment was done in TEM mode, we could not do accurate in-situ chemical measurements.

Therefore, the chemical changes occurring at the interface during the heating process were investigated on another lamella (see Fig. 1e, f) through doing in-situ heating test with no bias application. HAADF-STEM images + EELS chemical profiles (see Fig. S4 for position of STEM and EELS investigation) were acquired and the results are shown as Fig. 5. As seen, the chemical profiles are basically same for the nanostructures at room temperature and 500 °C indicating that no considerable chemical variation occurred. However, at 550 °C the oxygen (O) peak of

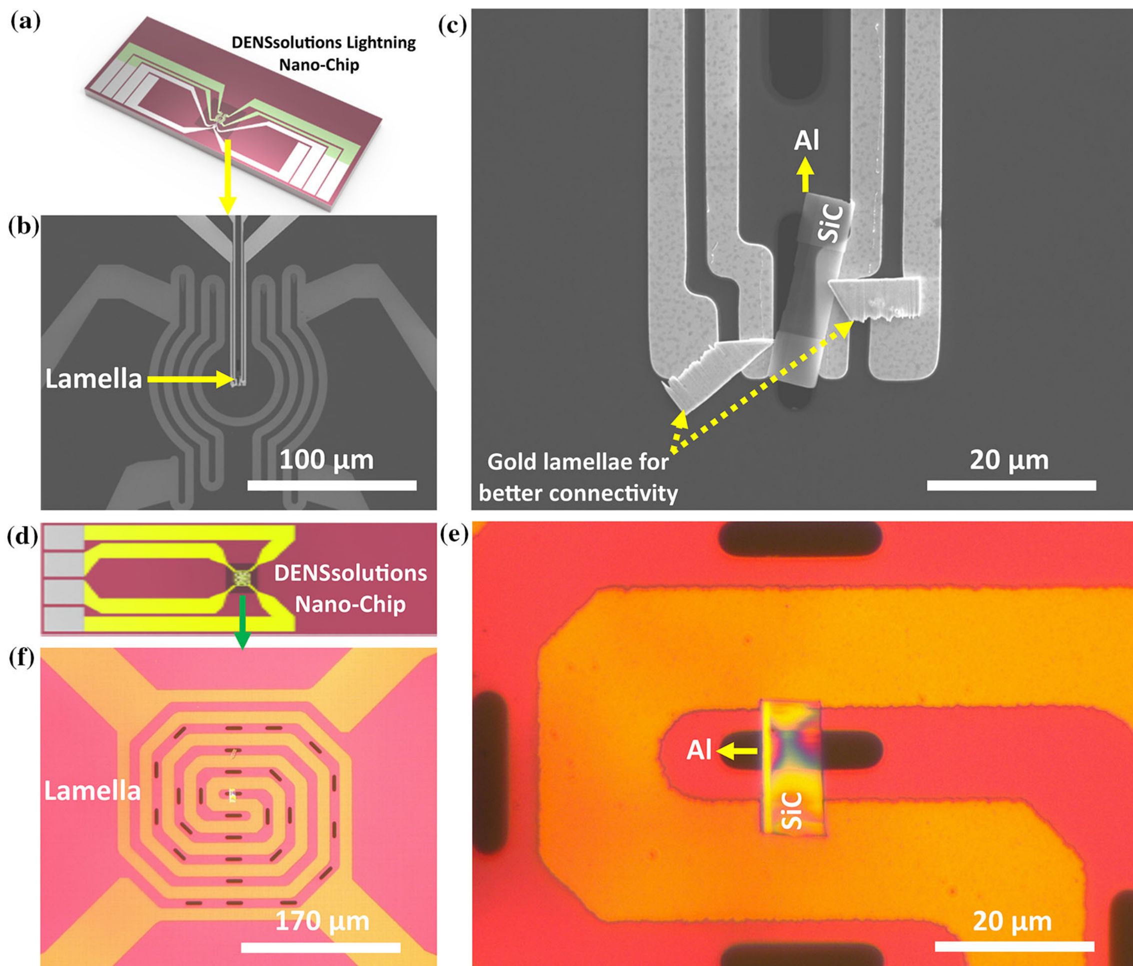

Figure 1 **a** DENSsolutions lightning nano-chip for in-situ biasing/heating experiment, **b** and **c** low- and high-magnification scanning electron microscopy (SEM) images of loaded lamella on chip, respectively. **d** DENSsolutions nano-chip for in-situ heating experiment, **e** and **f** low- and high-magnification optical microscopy (OM) images of loaded lamella, respectively.

AOL layer starts to flatten. At 600 °C oxygen seems to be uniformly spread in the AOL and Al phases, showing that O diffused in Al from AOL. Simultaneously the AOL width is reduced. Reduction of AOL width can be directly related to the decrease of the resistivity observed in the system (see I–V curves in Fig. 1). Recent nanoscale scanning spreading resistance microscopy analysis of SiO_2 amorphous layer/4H–SiC interface indicated that the carrier concentration in SiO_2 amorphous layer (10^{16} cm^{-3}) is three orders of magnitudes lower than 4H–SiC (10^{19} cm^{-3}) [40]. This is in same scale as the order of magnitude of resistivity drop observed in our experiment. It is well-known that O dissolution in Al is greatly limited at temperatures $\sim$ 660 °C (melting point of Al). Data collected by Wriedt [41] shows that only 2.9×10^{-8} at% of O can be dissolved in Al at its liquid state ($\sim$ 660 °C). The value for our system at 600 °C and at solid state will be slightly lower. Accordingly, it is expected that in Al side and at points close to the interface, alumina (Al_2O_3) forms and simultaneously Si is inserted in the Al [42]. Our line chemical profile with point resolution of 4 Å indicate significant change neither in the profile of Si nor Al in both sides of the device. Since the thickness of analyzed area is very thin (4 Å), there is a high possibility that such Si or Al_2O_3 formation occurred at other points near the interface.

Hence, the possibility of new phase formation was explored through analyzing the structural changes at the interface nanostructure. This was done using the BF (bright field)-STEM images (Fig. 6) of the corresponding HAADF-STEM images given in Fig. 5. The Fast Fourier Transformed (FFT) images of the

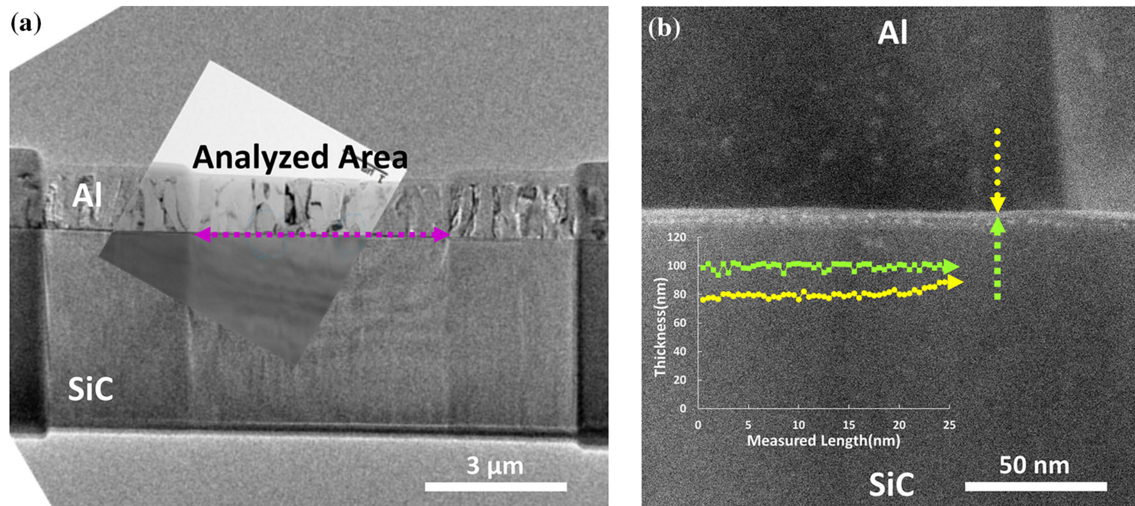

Figure 2 **a** Low-magnification bright field TEM image of prepared Al–AOL–SiC lamella, **b** High-magnification STEM image of Al–AOL–SiC interface. Inset in b shows thickness of lamella in Al and SiC areas. Lamella thickness was measured using EELS.

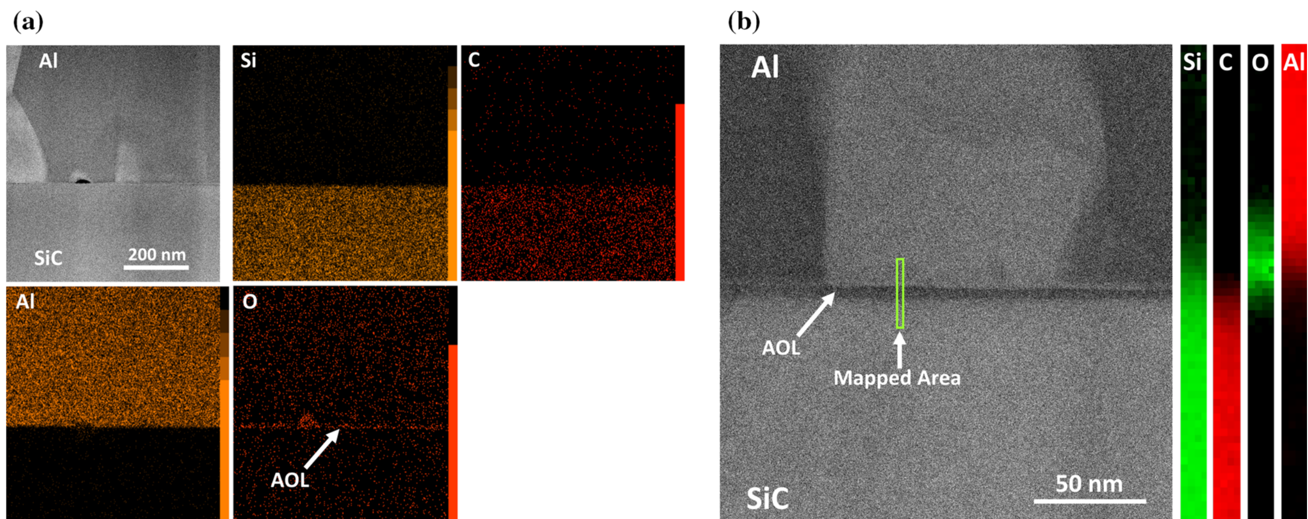

Figure 3 **a** EDS elemental mapping of Al–AOL–SiC interface, showing presence of AOL, **b** STEM-HAADF image of Al–AOL–SiC interface and its EELS map profile. Width and length of mapped area are 1.8 and 32 nm, respectively.

interface nanostructures are also presented in the Fig. 6. According to Figs. 6a, b and their FFTs, no additional phases were formed due to heating from room temperature to 500 °C. At 550 °C (Fig. 6c) the AOL thickness becomes smaller (~ 2 nm) and therefore Al and SiC grains will expand to occupy the AOL layer. Considering the initial thickness of Al (~ 1 µm) and SiC (~ 3.5 µm) layers and their thermal expansion coefficients, being 24×10^{-6} and 2.77×10^{-6} m/m °C [28], their expansions will be ~ 132 and 152 nm, respectively. At 600 °C (Fig. 6d) new reflections appear in the nanostructure. This is further investigated through inversing individual reflexes of each phase in the FFT pattern of Fig. 6d, and the results are shown as Fig. 7. In the IFFT images, the location of each phase can be found out through locating the brighter contrast. As seen, apart from the original phases (Al and SiC), there are now three new set of reflexes that belongs to Si, α-Al_2O_3 and Al_4C_3 phases. Si and α-Al_2O_3 are formed adjacent to one another in the Al side, while Al_4C_3 is formed adjacent to the interface in the SiC side. The fact that α-Al_2O_3 and Si are crystallized within the Al implies that AOL dissociates into its elemental form (Si and O), as is expected according to previous studies [43, 44]. After reaching to saturation level O

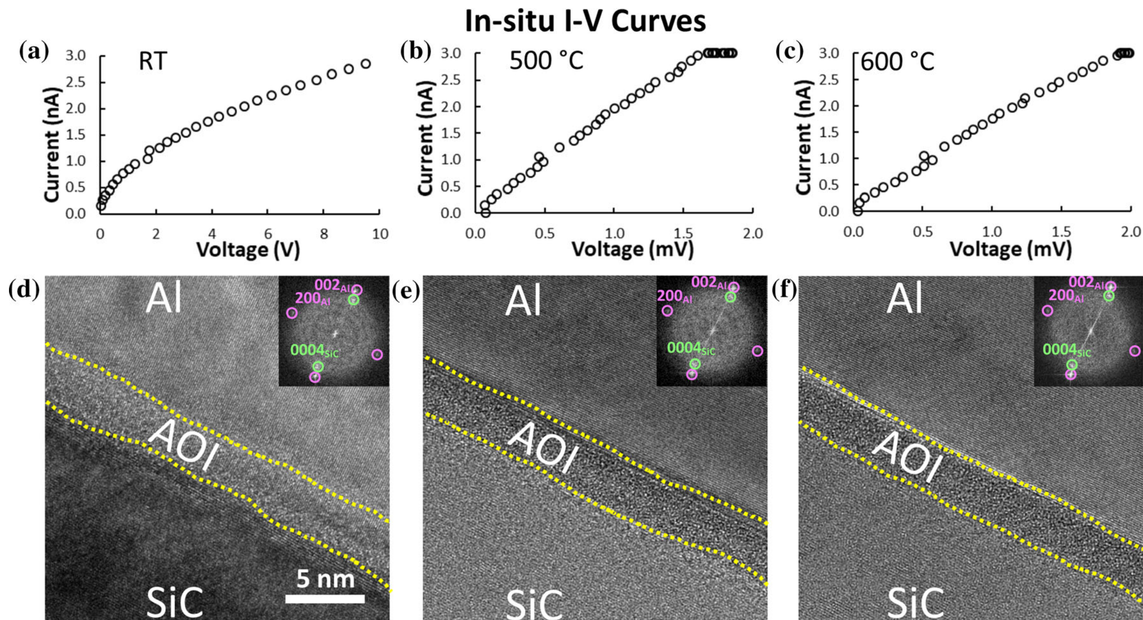

Figure 4 **a**, **b**, and **c** I–V curves of Al–AOL–SiC interface measured at room temperature (25°), 500° and 600 °C, respectively. **d**, **e**, and **f** high-magnification images of Al–AOL–SiC interface from a small area of low-magnification images (yellow squares in Fig. S2). FFT image of nanostructures shown in d, e, and f are presented as insets in same figures. Stacking of phases in all figures are similar (bottom: SiC, middle: AOL, top: Al). Scale bar in d applies also to **e** and **f**.

reacts with Al to form α-Al_2O_3, while Si will precipitate as Si nanocrystallite. In contrast to α-Al_2O_3 and Si, Al_4C_3 is formed within SiC with orientation relationship of $(0004)_{SiC}||(0006)_{Al4C3}$. The d-spacing of $(0006)_{Al4C3}$ was found to be ~ 4.00 Å, while according to Al_4C_3 structure it has to be 4.18 Å [45], indicating that Al_4C_3 nanocrystallite is possibly defective.

Discussions

As discussed before, the reaction of ceramics with metals can proceed through two different paths; (1) dissolution of the ceramic into the metal, and (2) elemental interdiffusion between the elements at the ceramic–metal interface. In the former, the elements from the ceramic dissolve into the metal and when the elements reach their saturation level the formation of new products occurs in the metal. In this study, since we observed the disappearance of AOL with increase in the temperature, and additionally Si and α-Al_2O_3 are formed in the Al, we infer that AOL, which is an amorphous phase, follows the first path. Such path for pure amorphous SiO_2 and consequent formation of Al_2O_3 and Si can be described as follows:

Step 1: Bond breakage

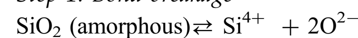

SiO_2 (amorphous) $\rightleftarrows Si^{4+} + 2O^{2-}$

Step 2: Dissolution

$Si^{4+} + 2O^{2-} \rightleftarrows Si_{dissolved\ in\ Al} + 2O_{dissolved\ in\ Al}$

Step 3: Reaction

$2Al + 3O_{dissolved\ in\ Al} \rightleftarrows Al_2O_3$

On the other hand, Al_4C_3 was formed within the SiC phase with a certain orientation relationship ($(0004)_{SiC}||(0006)_{Al4C3}$). In the previous research on a similar system (ex-situ TEM investigation on Al-

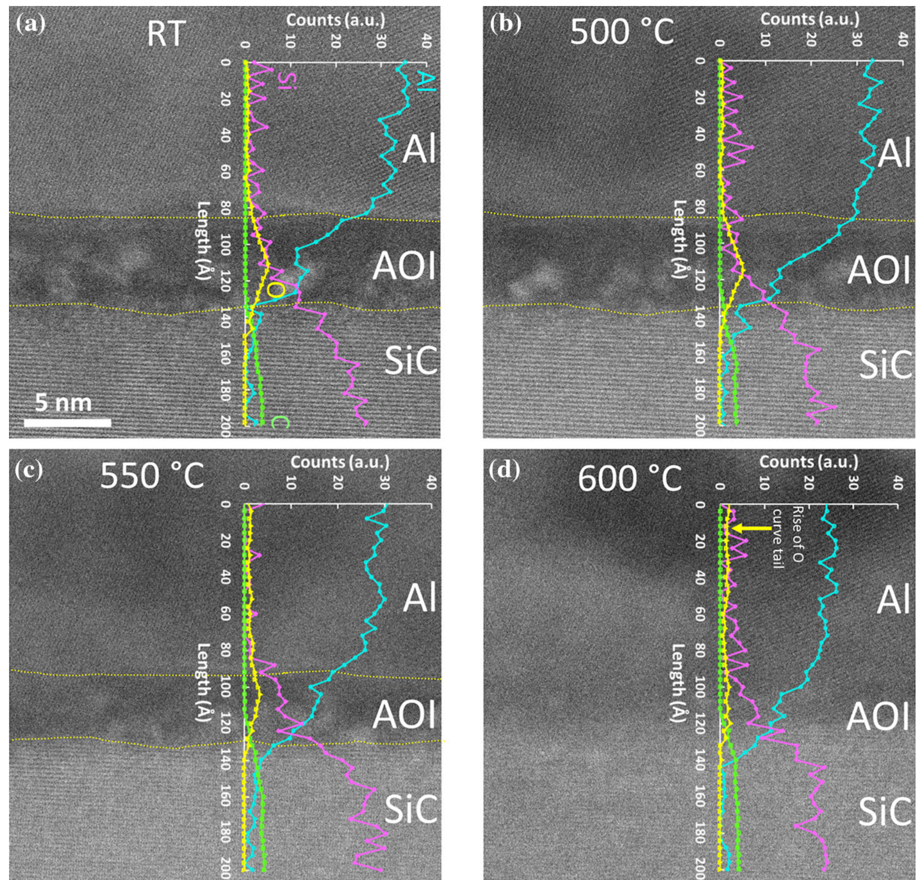

Figure 5 **a**, **b**, **c** and **d** show changes in chemistry (line profiles of Al (Aqua), Si (Violet), C (Lime), and O (Yellow)) of Al–AOL–SiC interface at room temperature (25°), 550°, 500° and 600 °C, respectively. White area in the AOL are Ga contamination due to FIB milling. Scale bar in a applies also to **b**, **c**, and **d**.

Si_3N_4 [33]), Adabifiroozjaei observed similar orientation relationship ($(0001)_{AlN} || (0001)_{Si3N4}$)) between the reaction product (AlN) and the ceramic reactant (Si_3N_4). Therefore, it was inferred that the reaction product is formed from the reactant through an elemental interdiffusion ($Al^{3+} \rightleftarrows Si^{4+}$) between the metal and the reactant ceramic. In fact, the ceramic reactant acted as a precursor for the reaction product, meaning that after interdiffusion the reactant transforms topotaxially to the reaction product, as this is observed in many ceramic systems with structural similarities [46]. In this study, the in-situ observation of the formation of Al_4C_3 within the SiC without destruction of SiC structure enabled us to conclude that in Al-SiC system interdiffusion of Al and Si at the interface is required to proceed the interfacial reaction. The interdiffusion path for reaction between Al and SiC involves three steps, as described below:

Step 1: Activation

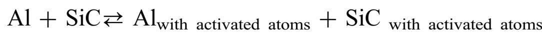

$$Al + SiC \rightleftarrows Al_{\text{with activated atoms}} + SiC_{\text{with activated atoms}}$$

Step 2: Interdiffusion

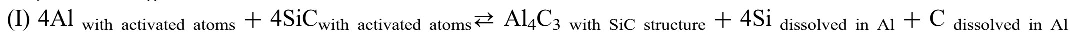

$$\text{(I) } 4Al_{\text{with activated atoms}} + 4SiC_{\text{with activated atoms}} \rightleftarrows Al_4C_{3\,\text{with SiC structure}} + 4Si_{\text{dissolved in Al}} + C_{\text{dissolved in Al}}$$

$$\text{Defect reaction: } 4Al_{Al}^{X} + 4Si_{Si}^{X} + 4C_{C}^{X} \rightleftarrows 4Al'_{\mathbf{Si\ in\ SiC}} + 3C^{X}_{\mathbf{c\ in\ SiC}} + V^{\bullet\bullet\bullet\bullet}_{\mathbf{C\ in\ SiC}} + 4Si^{\bullet}_{\mathbf{Al\ in\ Al}} + C''''_{\mathbf{i\ in\ Al}}$$

Step 3: Phase transformation

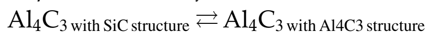

$$Al_4C_{3\,\text{with SiC structure}} \rightleftarrows Al_4C_{3\,\text{with Al4C3 structure}}$$

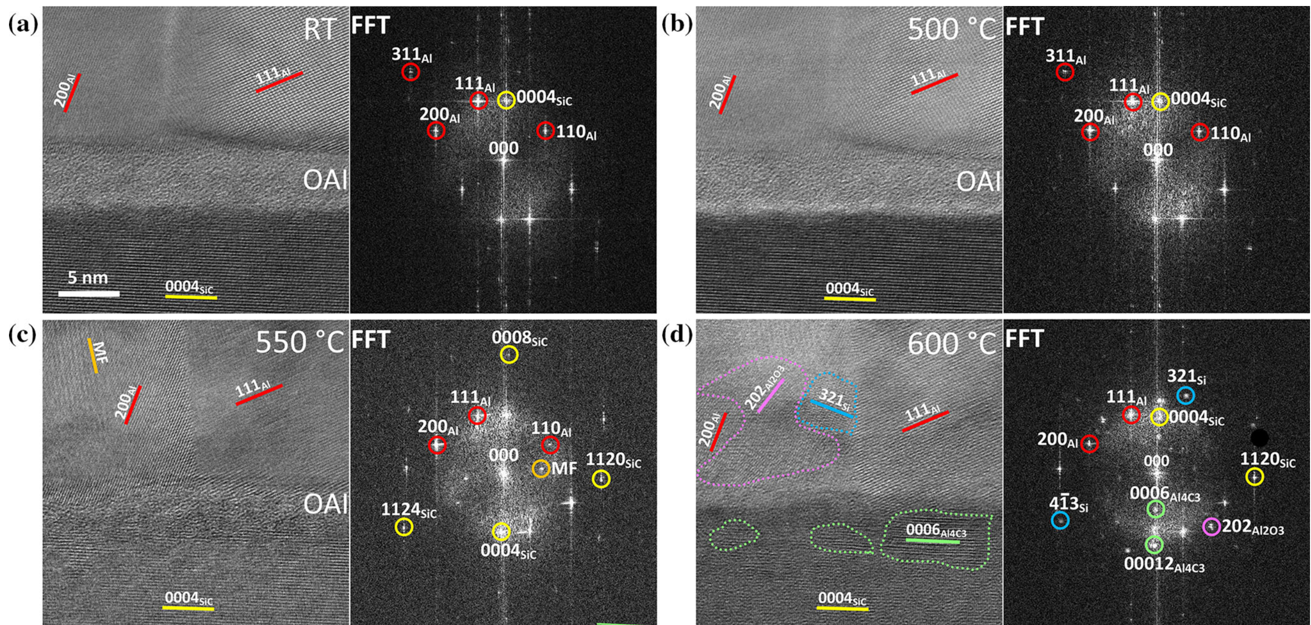

Figure 6 **a**, **b**, **c**, and **d** HRTEM and their corresponding FFT images of Al–AOL–SiC interface at room temperature (25°), 550°, 500° and 600 °C, respectively. Reflections of each phase are color-coded. MF in FFT of c stands for Moiré fringes that appears due to overlay of two Al grains at grain boundary area. Scale bar in a applies also to **b**, **c**, and **d**.

The observed difference between the *d*-spacing of Al_4C_3 crystallite characterized in the present study relative to perfect Al_4C_3 structure is due to the fact that there are some C vacancies ($V_{CinSiC}^{''''}$) in the Al_4C_3 crystallite as suggested by the above defect equilibria. This implies that the Step 3 (phase transformation) is not yet finished in the present study (Fig. 6d). It is expected that when Step 3 is finished, due to density difference of Al_4C_3 (2.93 g/cm^3) and SiC (3.16 g/cm^3), the former gets separated from the latter as a nanocrystallite with distinct boundaries. At the end, when heat-treatment process is continued for considerable amount of time, these nanocrystallites will join and form larger grains that might or might not have orientation relationship with the reactant ceramic [25, 28].

Our results clearly show that SiO_2 amorphous phase has different reaction mechanism with Al than the crystalline SiC. As mentioned before, the current theories suggest that reaction between metals and ceramics can either follow the dissolution [22, 23, 28, 47] or the interdiffusion path [33–38]. The reason behind the different reaction mechanism for SiO_2 amorphous phase and SiC can be explained using the structural similarities of reaction products and the reactants for the crystalline ceramics. This was hypothesized in the previous study on crystalline oxides ($CaAl_2Si_2O_8$–Al system [35]) and subsequently was applied to the Al–Si_3N_4 system [33]. In Ref. [35], it is suggested that because of close structural similarity between the reactant ceramic ($CaAl_2Si_2O_8$) and the reaction product ($CaAl_4O_7$), the

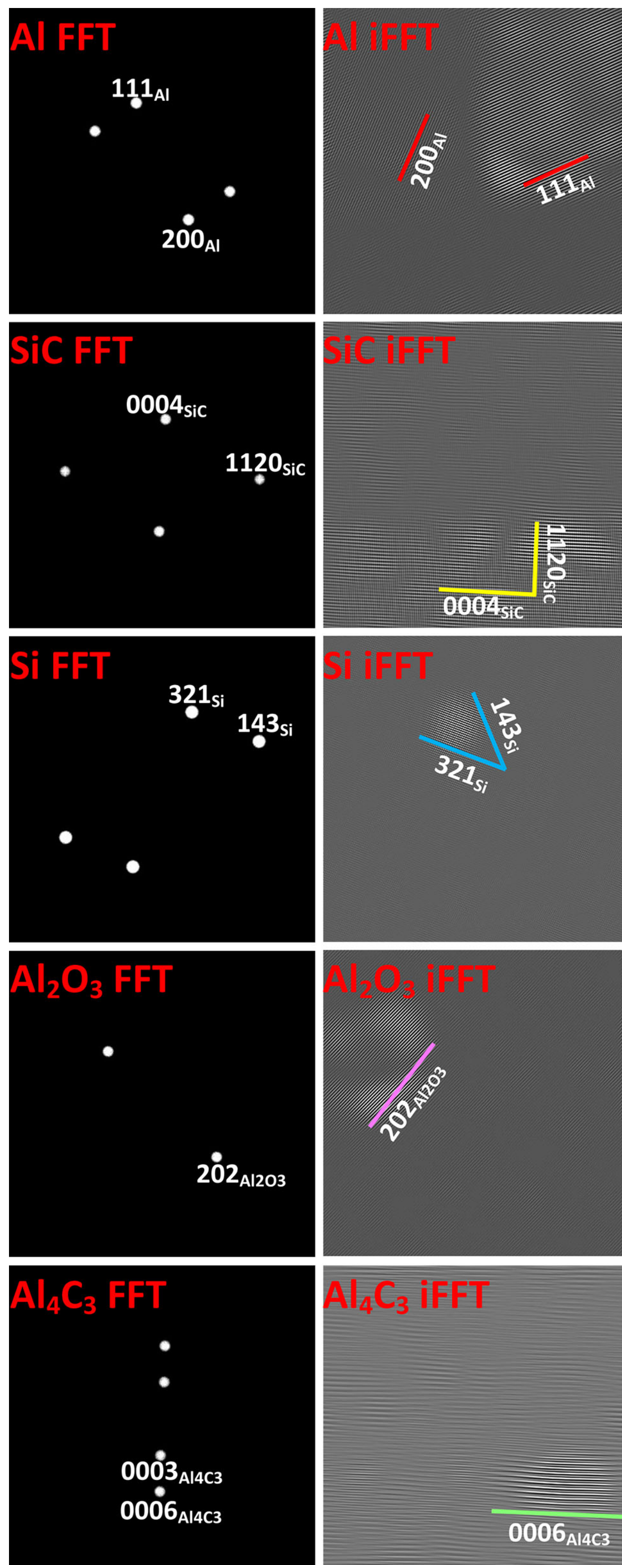

Figure 7 Phase configuration observed in Fig. 6d, deconvoluted using FFT and inverse FFT images.

space group of the latter ($C2/c$) being subgroup of the space group of the former ($P\bar{1}$)), then $CaAl_4O_7$ is merely formed through an elemental interdiffusion ($Al^{3+} \rightleftarrows Ca^{2+}$ and $Al^{3+} \rightleftarrows Si^{4+}$) between $CaAl_2Si_2O_8$ and Al. This is particularly relevant when the cations in the metal and ceramics are not very different in their sizes (*e.g.* Si crystal radius: 0.4 Å and Al crystal radius: 0.53 Å), as they create nearly same surrounding environment with common anion (*e.g.* C, N, or O). Regarding Al-SiC system, Fig. 8 presents similarities of the atomic arrangement of SiC (reactant) and Al_4C_3 (reaction product). The arrangement of the cations (Al and Si) in both structures is very alike. Further, the lattice parameters of SiC ($a = b = 3.079$ Å, $c = 10.082$ Å) and Al_4C_3 ($a = b = 3.354$ Å, $c = 25.116$ Å), and space groups (SiC: $P6_3mc$, Al_4C_3: R3m) are very close. c in Al_4C_3 is $\sim$ 2.5 larger than c in SiC. Therefore, the similarity of the structures paves the way for reaction to proceed through elemental interdiffusion. On the other hand, the dissociation occurs for AOL since there does not exist such structural similarities between α-Al_2O_3 and AOL (amorphous SiO_2).

Conclusion

Through careful device preparation of a representative reactive metal-ceramic system (Al–AOL–SiC) and consequent presentation of a comprehensive ultrahigh-resolution electrical, chemical and structural data aqcuired by in-situ TEM and STEM techniques we elaborate that reaction mechanisms between Al and SiO_2 amorphous layer is different from that between Al and SiC. The reaction between SiC and Al proceed through elemental interdiffusions, while that between SiO_2 and Al follows the dissolution mechanism. Additionally, we hypothesize that the elemental diffusions are encouraged due to similarities of atomic arrangements in the reactant (SiC) and reaction product (Al_4C_3) structures. Our findings might be applicable to other reactive metals-crystalline ceramics systems that are currently used in manufacturing and electronic industries.

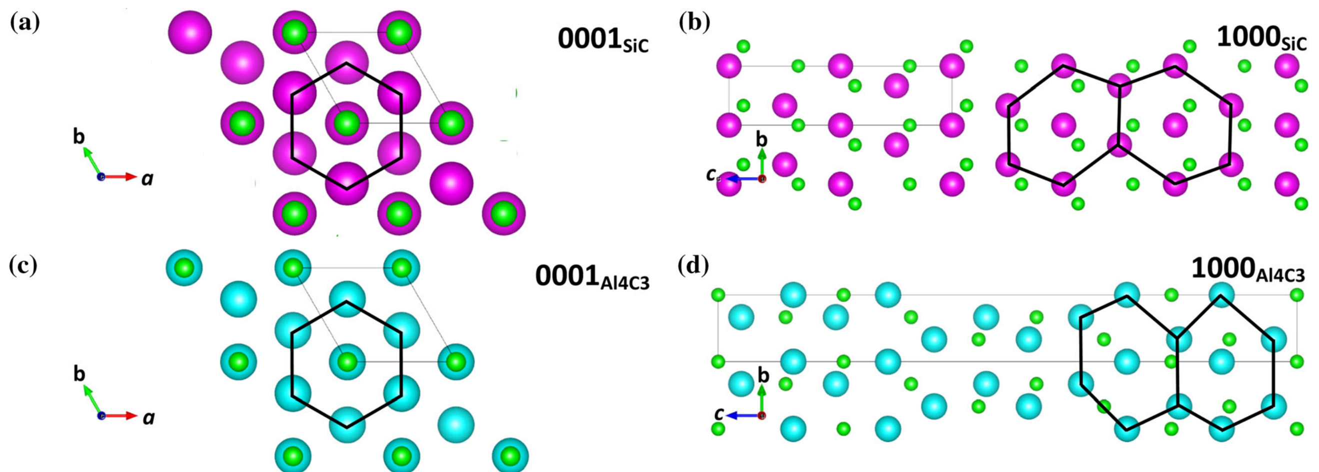

Figure 8 **a** and **b** SiC structures in [0001] and [1000] directions, respectively, and **c** and **d** Al_4C_3 structures in [0001] and [1000] directions, respectively. SiC structure is 2 × 2 × 2.5 supercell, while that of Al_4C_3 is a 2 × 2 × 1 supercell. Al (Aqua), Si (Violet), C (Lime). Hexagons are superimposed on structures to show similarities of atomic arrangements. Structures are visualized using VESTA visualization program.

Acknowledgements

E.A. acknowledges financial support of Japanese Society for Proposition of Science (JSPS KAKENHI Grant Number JP18F18064). E.A. also acknowledges Electron Microscopy Analysis Station of National Institute for Materials Science (NIMS) for provision of their resources. L.M.-L. acknowledges European Research Council (ERC) "Horizon 2020" Program under Grant No. 805359-FOXON.

Funding

Open Access funding enabled and organized by Projekt DEAL.

Data availability

The data used in this study are available from the corresponding author (e.adabifiroozjaei@aem.tu-darmstadt.de) upon reasonable request.

Declarations

Competing interests The authors declare no competing interests.

Supplementary Information: The online version contains supplementary material available at https://doi.org/10.1007/s10853-023-08186-z.

Open Access This article is licensed under a Creative Commons Attribution 4.0 International License, which permits use, sharing, adaptation, distribution and reproduction in any medium or format, as long as you give appropriate credit to the original author(s) and the source, provide a link to the Creative Commons licence, and indicate if changes were made. The images or other third party material in this article are included in the article's Creative Commons licence, unless indicated otherwise in a credit line to the material. If material is not included in the article's Creative Commons licence and your intended use is not permitted by statutory regulation or exceeds the permitted use, you will need to obtain permission directly from the copyright holder. To view a copy of this licence, visit http://creativecommons.org/licenses/by/4.0/.

Supplementary Information: The online version contains supplementary material available at https://doi.org/10.1007/s10853-023-08186-z.

References

[1] Kumar A, Barda H, Klinger L et al (2018) Anomalous diffusion along metal/ceramic interfaces. Nat Commun 9:5251. https://doi.org/10.1038/s41467-018-07724-7

[2] Yang C, Hu C, Xiang C et al (2021) Interfacial superstructures and chemical bonding transitions at metal-ceramic interfaces. Sci Adv 7:eabf6667. https://doi.org/10.1126/sciadv.abf6667

[3] Kingery WD (1953) Metal-ceramic interactions: I, factors affecting fabrication and properties of cermet bodies. J Am Ceram Soc 36:362–365. https://doi.org/10.1111/j.1151-2916.1953.tb12818.x

[4] Caccia M, Tabandeh-Khorshid M, Itskos G et al (2018) Ceramic–metal composites for heat exchangers in concentrated solar power plants. Nature 562:406–409. https://doi.org/10.1038/s41586-018-0593-1

[5] Kumamoto A, Shibata N, Nayuki K et al (2016) Atomic structures of a liquid-phase bonded metal/nitride heterointerface. Sci Rep 6:22936. https://doi.org/10.1038/srep22936

[6] Wen Z, Li C, Wu D et al (2013) Ferroelectric-field-effect-enhanced electroresistance in metal/ferroelectric/semiconductor tunnel junctions. Nat Mater 12:617–621. https://doi.org/10.1038/nmat3649

[7] Rühle M (1997) Microscopy of structural ceramics. Adv Mater 9:195–217. https://doi.org/10.1002/adma.19970090304

[8] Baram M, Chatain D, Kaplan WD (2011) Nanometer-thick equilibrium films: the interface between thermodynamics and atomistics. Science 332:206–209. https://doi.org/10.1126/science.1201596

[9] Banger KK, Yamashita Y, Mori K et al (2011) Low-temperature, high-performance solution-processed metal oxide thin-film transistors formed by a 'sol–gel on chip' process. Nat Mater 10:45–50. https://doi.org/10.1038/nmat2914

[10] Porter LM, Davis RF (1995) A critical review of ohmic and rectifying contacts for silicon carbide. Mater Sci Eng B 34:83–105. https://doi.org/10.1016/0921-5107(95)01276-1

[11] Suzuki A, Ashida H, Furui N et al (1982) Thermal oxidation of SiC and electrical properties of Al–SiO_2–SiC MOS structure. Jpn J Appl Phys 21:579–585. https://doi.org/10.1143/JJAP.21.579

[12] Fiorenza P, Iucolano F, Nicotra G et al (2018) Electron trapping at SiO2/4H–SiC interface probed by transient capacitance measurements and atomic resolution chemical analysis. Nanotechnology 29:395702. https://doi.org/10.1088/1361-6528/aad129

[13] Lin T-C, Cao C, Sokoluk M et al (2019) Aluminum with dispersed nanoparticles by laser additive manufacturing. Nat Commun 10:4124. https://doi.org/10.1038/s41467-019-12047-2

[14] Kim S-M, Koo S-M (2018) Electrical properties of Al/Al_4C_3/4H–SiC diodes. Mater Sci Semicond Process 74:170–174. https://doi.org/10.1016/j.mssp.2017.10.012

[15] Kim Y, Lee J-C (2006) Processing and interfacial bonding strength of 2014Al matrix composites reinforced with oxidized SiC particles. Mater Sci Eng A 420:8–12. https://doi.org/10.1016/j.msea.2005.12.032

[16] Gu M, Jin Y, Mei Z et al (1998) Effects of reinforcement oxidation on the mechanical properties of SiC particulate reinforced aluminum composites. Mater Sci Eng A 252:188–198. https://doi.org/10.1016/S0921-5093(98)00674-1

[17] Huang L, Xia M, Gu X (2020) A critical review of theory and progress in Ohmic contacts to p-type SiC. J Cryst Growth 531:125353. https://doi.org/10.1016/j.jcrysgro.2019.125353

[18] Harrell WR, Zhang J, Poole KF (2002) Aluminum schottky contacts to n-type 4H–SiC. J Electron Mater 31:1090–1095. https://doi.org/10.1007/s11664-002-0047-1

[19] Kyoung S, Jung E-S, Sung MY (2016) Post-annealing processes to improve inhomogeneity of Schottky barrier height in Ti/Al 4H–SiC Schottky barrier diode. Microelectron Eng 154:69–73. https://doi.org/10.1016/j.mee.2016.01.013

[20] Fernie JA, Drew RAL, Knowles KM (2009) Joining of engineering ceramics. Int Mater Rev 54:283–331. https://doi.org/10.1179/174328009X461078

[21] Gu M, Mei Z, Jin Y, Wu Z (1999) Structure and amorphization of the oxide on the silicon carbide surface in an SiCp/Al composite. Scr Mater 40:985–991. https://doi.org/10.1016/S1359-6462(99)00006-8

[22] Eustathopoulos N (2005) Progress in understanding and modeling reactive wetting of metals on ceramics. Curr Opin Solid State Mater Sci 9:152–160. https://doi.org/10.1016/j.cossms.2006.04.004

[23] Eustathopoulos N, Voytovych R (2016) The role of reactivity in wetting by liquid metals: a review. J Mater Sci 51:425–437. https://doi.org/10.1007/s10853-015-9331-3

[24] Raghavan V (2008) Al–C–Si (Aluminum-Carbon-Silicon). J Phase Equilibria Diffus 29:365–366. https://doi.org/10.1007/s11669-008-9332-x

[25] Kaplan WD, Chatain D, Wynblatt P, Carter WC (2013) A review of wetting versus adsorption, complexions, and related phenomena: the Rosetta stone of wetting. J Mater Sci 48:5681–5717. https://doi.org/10.1007/s10853-013-7462-y

[26] Dillon SJ, Tang M, Carter WC, Harmer MP (2007) Complexion: a new concept for kinetic engineering in materials science. Acta Mater 55:6208–6218. https://doi.org/10.1016/j.actamat.2007.07.029

[27] Chua AL-S, Benedek NA, Chen L et al (2010) A genetic algorithm for predicting the structures of interfaces in multicomponent systems. Nat Mater 9:418–422. https://doi.org/10.1038/nmat2712

[28] Howe JM (1993) Bonding, structure, and properties of metal/ceramic interfaces: part 1 chemical bonding, chemical reaction, and interfacial structure. Int Mater Rev 38:233–256. https://doi.org/10.1179/imr.1993.38.5.233

[29] Jeurgens LPH, Wang Z, Mittemeijer EJ (2009) Thermodynamics of reactions and phase transformations at interfaces and surfaces. Int J Mater Res 100:1281–1307. https://doi.org/10.3139/146.110204

[30] Badami DV (1962) Graphitization of α-silicon carbide. Nature 193:569–570. https://doi.org/10.1038/193569a0

[31] Charrier A, Coati A, Argunova T et al (2002) Solid-state decomposition of silicon carbide for growing ultra-thin heteroepitaxial graphite films. J Appl Phys 92:2479–2484. https://doi.org/10.1063/1.1498962

[32] Romero JC, Arsenault RJ (1995) Anomalous penetration of Al into SiC. Acta Metall Mater 43:849–857. https://doi.org/10.1016/0956-7151(94)00250-L

[33] Adabifiroozjaei E, Koshy P, Emadi F et al (2019) Ionic interdiffusion as interaction mechanism between Al and Si_3N_4. J Am Ceram Soc 102:4835–4847. https://doi.org/10.1111/jace.16358

[34] Adabifiroozjaei E, Ma H, Koshy P, Sorrell CC (2017) Anorthite ($CaAl_2Si_2O_8$)–aluminum interface: kinetics of high-temperature interactions. J Mater Sci 52:6767–6777. https://doi.org/10.1007/s10853-017-0913-0

[35] Adabifiroozjaei E, Koshy P, Rastkerdar E, Sorrell CC, (2016) Interfacial reactions between anorthite ($CaAl_2Si_2O_8$) and Al 7075 Alloy at 850 °C and 1150 °C. J Am Ceram Soc 99:1694–1708. https://doi.org/10.1111/jace.14091

[36] Adabifiroozjaei E, Koshy P, Pardehkhorram R et al (2015) Interfacial reactions between $BaAl_2Si_2O_8$ and molten Al alloy at 850 °C. J Am Ceram Soc 98:3299–3307. https://doi.org/10.1111/jace.13650

[37] Adabifiroozjaei E, Koshy P, Pardehkhorram R et al (2016) Interfacial reactions between $BaAl_2Si_2O_8$ and molten Al alloy at 1423 K and 1523 K (1150 °C and 1250 °C). Metall Mater Trans B 47:1753–1764. https://doi.org/10.1007/s11663-016-0642-9

[38] Raj R, Saha A, An L et al (2002) Ion exchange at a metal–ceramic interface. Acta Mater 50:1165–1176. https://doi.org/10.1016/S1359-6454(01)00418-9

[39] Saiz E, Cannon RM, Tomsia AP (2000) Enhanced atomic transport at liquid metal/Al_2O_3 interfaces. Adv Mater 12:1952–1955. https://doi.org/10.1002/1521-4095(200012)12:24%3c1952::AID-ADMA1952%3e3.0.CO;2-#

[40] Fiorenza P, Giannazzo F, Vivona M et al (2013) SiO_2/4H–SiC interface doping during post-deposition-annealing of the oxide in N_2O or $POCl_3$. Appl Phys Lett 103:153508. https://doi.org/10.1063/1.4824980

[41] Wriedt HA (1985) The Al–O (Aluminum-Oxygen) system. Bull Alloy Phase Diagr 6:548–553. https://doi.org/10.1007/BF02887157

[42] Laurent V, Chatain D, Eustathopoulos N (1991) Wettability of SiO_2 and oxidized SiC by aluminium. Mater Sci Eng A 135:89–94. https://doi.org/10.1016/0921-5093(91)90542-U

[43] Prabriputaloong K, Piggott MR (1973) Reduction of SiO_2 by molten Al. J Am Ceram Soc 56:184–185. https://doi.org/10.1111/j.1151-2916.1973.tb12451.x

[44] Standage AE, Gani MS (1967) Reaction between vitreous silica and molten aluminum. J Am Ceram Soc 50:101–105. https://doi.org/10.1111/j.1151-2916.1967.tb15049.x

[45] The Materials Project (2020) Materials data on Al_4C_3 by materials project. Database version v2022.10.28 (mp-743752). https://doi.org/10.17188/1288073

[46] Glasser LSD, Glasser FP, Taylor HFW (1962) Topotactic reactions in inorganic oxy-compounds. Q Rev Chem Soc 16:343–360. https://doi.org/10.1039/QR9621600343

[47] Weil KS (2013) Fundamentals and methods of ceramic joining. Ceramics science and technology. John Wiley & Sons Ltd, New york, pp 215–246

Publisher's Note Springer Nature remains neutral with regard to jurisdictional claims in published maps and institutional affiliations.